Pinning properties and vortex dynamics in thin superconducting films with ferromagnetic and antiferromagnetic arrays of magnetic dots

Q. H. Chen, G. Teniers, B. B. Jin, and V. V. Moshchalkov*
Nanoscale Superconductivity and Magnetism Group, Division of Solid State Physics and Magnetism, Katholieke Universiteit Leuven, Celestijnenlaan 200 D, B-3001 Leuven, Belgium
(Received 17 June 2005; revised manuscript received 8 September 2005; published 9 January 2006)

We report on the simulations of the pinning properties and vortex dynamics in thin superconducting film with three different periodic arrays of magnetic dots: (1) all magnetic dots have the same magnetization orientation (ferromagnetic pinning array); (2) magnetic dots with up and down magnetization orientation are arranged alternatively, to form an antiferromagnetic two-dimensional array; and (3) the same as the previous array, but each dot is replaced by a 2×2 magnetic dot subarray. All dots in the subarray have the same magnetization orientation. We calculated the critical depinning force and magnetization as a function of the applied magnetic field for these three arrays. Due to the field polarity-dependent flux pinning effect of the magnetic dots, asymmetric pinning behavior in the first array can be switched to the symmetric one in the latter two arrays while keeping the pronounced matching effects. We also calculated the current-voltage characteristics at both commensurate and incommensurate fields. We found that at the first matching field, the transition from the pinned phase to a vortex motion phase is continuous for the ferromagnetic configuration but discontinuous for the two antiferromagnetic configurations. This can be explained by different vortex dynamical trajectories. Our results indicate that pinning properties and vortex dynamics in thin superconducting films can be manipulated by tuning the configuration of the magnetic dot array.

DOI: 10.1103/PhysRevB.73.014506 PACS number(s): 74.78.Na, 74.25.Sv, 74.25.Qt

I. INTRODUCTION

Pinning properties and vortex dynamics of thin superconducting (SC) films with artificial periodic pinning arrays have drawn great attention in the past decades.[1–17] Such arrays are usually composed of nanoscale antidots or magnetic dots with a diameter significantly smaller than the spacing between them. The antidots and magnetic dots act as pinning sites to trap the vortices and are able to change the vortex lattice symmetry. Magnetization and transport measurements have clearly demonstrated the presence of commensurability or matching effects between the vortex lattice and the pinning array when the density of the vortices equals an integer or fractional multiple of the density of the pinning sites.[1–3,6–10] These effects were also reproduced in numerical simulations.[12–17]

However, the distinction between the flux pinning properties of the antidot and magnetic dot arrays was clearly revealed in the magnetization measurements.[1,8–10] SC films with magnetic dot arrays produce magnetization loops which are asymmetrical with respect to the field polarity, in contrast to the usual symmetric shape of the magnetization loops of films with the antidot arrays. This has been attributed to the field polarity-dependent flux pinning effect of the magnetic dots, i.e., their pinning properties are dependent on the mutual orientation between the out-of-plane magnetization of the magnetic dots and the magnetic field (H) applied perpendicular to the film.[8–10] The magnetic dot can produce an *attractive* pinning potential when H is parallel to the magnetic moment of the dot and *repulsive* when H is antiparallel to it. This asymmetry between positive and negative field polarity has been successfully reproduced in numerical simulations, which explicitly take into account the field polarity-dependent flux pinning effect.[17] This effect has been used in the simulation to tune the pinning properties of thin SC films. A square magnetic dot array with *random* distribution of the *antiparallel* magnetic dot moments, which is different from the one used in experiments with a unique magnetized orientation of all dots, was also attempted in Ref. 17. Unfortunately, the obtained results showed quite weak matching effects, far away from the expectation for improving the pinning properties. Therefore, more simulation work is necessary to find a new configuration for better pinning properties.

In the present work we simulated the pinning properties and vortex dynamics of thin SC films with three kinds of periodic magnetic dot arrays. These three arrays have regular distributions of the magnetic moments (both ferromagnetic and antiferromagnetic distribution), which are different from the random distribution used in the previous simulation.[17] In addition, in our simulations we used more realistic magnetic-field profiles of the magnetic dot, instead of the dipole approximation. The simulated pinning property results have clearly demonstrated that among the different arrays, due to the field polarity-dependent flux pinning effect of the magnetic dot, the asymmetric pinning behavior can be switched to the symmetric one while keeping pronounced matching effects. The vortex patterns at certain matching and submatching fields are also analyzed in this work in order to understand the microscopic origin of the observed switching. We also calculated the current-voltage (I-V) characteristics for these three configurations of the magnetic dots. Most of the I-V curves are similar to those reported in previous publications.[15,16] But, we found, at the matching field, a continuous transition from the pinned phase to a moving phase for the ferromagnetic dot array, while discontinuous for the

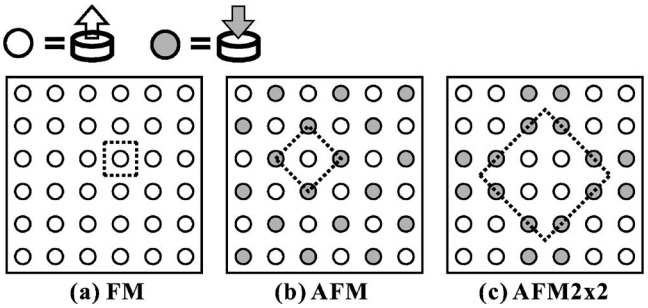

FIG. 1. Three configurations of the magnetic dot arrays used in our simulation: (a) FM, (b) AFM, and (c) AFM2×2. The black open and gray filled circles are the up- and down-magnetized dots. The dotted lines indicate the unit cells for each configuration.

two antiferromagnetic configurations. This difference has been attributed to the presence of specific trajectories of the depinned vortices. Our results demonstrate that the pinning properties and vortex dynamics can be tuned by using proper arrangements of the magnetic dot arrays.

II. FERROMAGNETIC AND ANTIFERROMAGNETIC ARRAYS OF MAGNETIC DOTS

We used in our simulations three different periodic magnetic dot arrays shown in Fig. 1. The magnetic dots with out-of-plane magnetization have two kinds of orientation, "up" and "down." The unit cell for each periodic array is indicated by the dotted lines. Figure 1(a) shows the ferromagnetically ordered array of the dots. The unit cell is a square, containing one up-magnetized dot. In the second configuration, as shown in Fig. 1(b), the dots are ordered to form an antiferromagnetic two-dimensional (2D) array. The unit cell is a square rotated by 45°. The third configuration is similar to the second one, but each dot is replaced by a 2×2 cell with four dots of the same orientation, as seen in Fig. 1(c). The unit cell includes four up- and four down-magnetized dots. The latter two configurations have an antiferromagnetic order, which is quite different from a random distribution of magnetic moments used in the previous simulation.[17] In the following these three configurations are called FM (ferromagnetic), AFM (antiferromagnetic), and AFM2×2, respectively.

III. SIMULATION

We consider a two-dimensional vortex system and model the vortex motion with overdamped Langevin dynamics.[12–17] The total force acting on vortex i is given by

$$\vec{F}_i = \vec{F}^L + \vec{F}_i^{vv} + \vec{F}_i^{vp} + \vec{F}^T - \eta\vec{v}_i = 0, \tag{1}$$

where $\vec{F}^L$ is the Lorentz force acting equally on all vortices, $\vec{F}_i^{vv}$ is the vortex-vortex interaction force from all other vortices, $\vec{F}_i^{vp}$ is the vortex-pinning interaction force from all pinning sites, and $\vec{F}^T$ is a stochastic noise term to model the temperature effect; η is the viscosity coefficient, taken to be unity, and $\vec{v}_i$ is the velocity of vortex i. In our simulation $\vec{F}_i^{vv}$ is modeled by the interaction force between the Pearl vortices[17–20]

$$\vec{F}_i^{vv} = -\sum_{j\neq i}^{N_v} \nabla\left(\int \frac{d^2\vec{k}}{4\pi^2} E_0 \frac{2\pi t}{k^2 + k\Lambda^{-1}} e^{i\vec{k}\cdot\vec{r}_{ij}}\right), \tag{2}$$

where N_v is the number of the vortices, $\vec{r}_{ij}$ is the displacement vector between vortex i and vortex j, t is the thickness of the SC film, Λ is the effective penetration depth which is equal to $2\lambda^2/t$, and $E_0=\Phi_0^2/(2\pi\mu_0\lambda^2)$ is the energy constant (energy per length). Here λ is the London penetration depth, Φ_0 is the flux quantum, and μ_0 is the vacuum permeability. The repulsive forces from all other vortices are included because of their long-range character. A smoothed method[21,22] is introduced here to deal with such interaction, which is of a look-up-table up to distance 100 Λ by 0.04 Λ step and an interpolation item for distance longer than 100 Λ. In the case of magnetic dots with out-of-plane magnetization, $\vec{F}_i^{vp}$ is modeled as[23]

$$\vec{F}_i^{vp} = -\sum_{k}^{N_m} \frac{MR\Phi_0^2}{\lambda^2} \int_0^\infty dq \frac{1}{Q} J_1(qR) J_1(q\rho_{ik}) E(q,l,D), \tag{3}$$

where N_m is the number of the magnetic dots, $Q=p[p+q\coth(pt/2)]$ with $p=\sqrt{1+q^2}$, $E(q,l,D)=e^{-ql}(e^{-qD}-1)$, $J_1(x)$ is the Bessel function, and l is the distance between the bottom of the SC film and the upper surface of the dot (in experiments, SC film is usually deposited on top of the magnetic dots with an insulating layer in between to avoid proximity effects[8–10]). R and D are the radius and thickness of the dots, respectively, ρ_{ik} is the distance between the vortex i and the mapping center of the magnetic dot on SC films, and M is the magnetization with $M=m/(\pi R^2 D)$ (in units of $M_0=\Phi_0/\lambda^2$), where m is the total magnetic moment of a dot. When the magnetic moment and the flux of the vortex have the same polarity (parallel configuration), the interaction force is attractive; however, if they have the opposite polarity (antiparallel configuration), the interaction force is repulsive. The pinning center-vortex force $\vec{F}_i^{vp}$ is a short-range interaction. It decreases as ρ_{ik}^{-4} at distances larger than the magnetic dot lattice constant a, and we use the cutoff assuming that the force is negligible for distances greater than a. The forces in Eqs. (1)–(3) are all in units of $f_0=\Phi_0^2/\lambda^3$, where f_0 is force per unit length. Unlike previous calculations,[17] we consider here the finite size effect of the magnetic dots, which is more realistic and closer to the practical situation.

The parameters used in our simulations are set to $\lambda=200$ nm, $t=75$ nm, $l=40$ nm, $R=200$ nm, and $d=20$ nm. We also chose the magnetization M as $50M_0$ in this work. So, the largest pinning strength f_p, which is realized at the edge of a dot,[23] is taken to be equal to $0.279\,22 f_0$. The lattice constant a of the pinning arrays is 1.5 Λ, yielding the pinning site density of $4/(9\ \Lambda^2)$. We supposed that only one flux quantum can be pinned at each pinning site and no multiquanta vortices can be formed at the magnetic dots during the simulations. We imposed periodic boundary conditions on our virtual samples. The sample sizes are $18\times 18\ \Lambda^2$ in calculating critical depinning force and current-voltage characteristics. The vortices are first introduced randomly at each

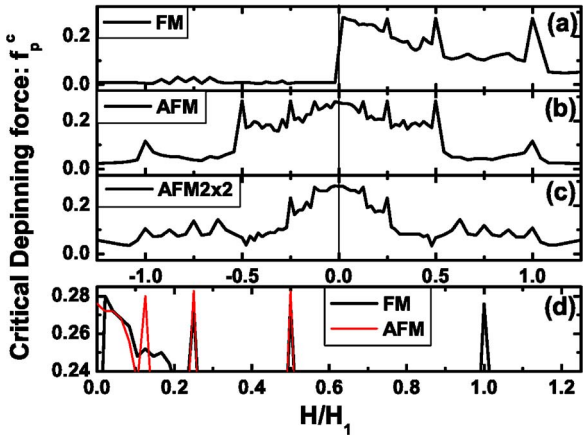

FIG. 2. (Color online) Critical depinning force f_p^c as a function of the applied magnetic field H for the three configurations: (a) FM, (b) AFM, and (c) AFM2×2. The field polarity-dependent asymmetric pinning is clearly seen for the FM configuration, and symmetric pinning for the AFM and AFM2×2 configurations. (d) is a comparison of the peaks at positive field between the FM and AFM configurations.

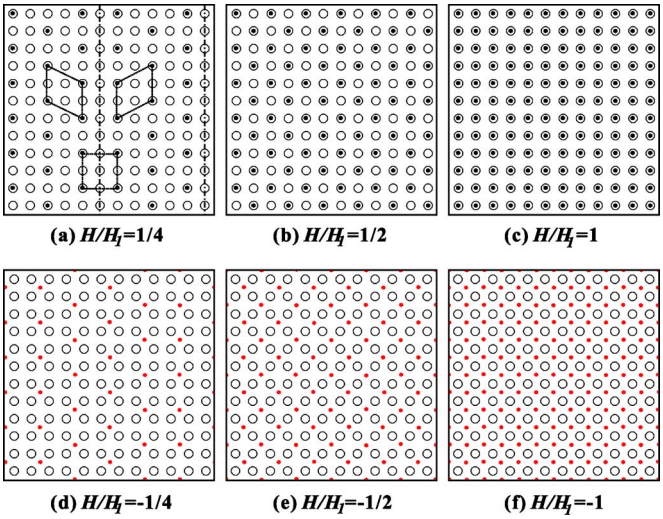

FIG. 3. (Color online) Vortex patterns for the FM configuration at (a) $H/H_1=1/4$, (b) 1/2, (c) 1, (d) −1/4, (e) −1/2, and (f) −1. The solid dots in upper and lower panels are the vortices and antivortices, respectively. The dashed dotted lines indicate the domain walls, which are due to the small difference in energy between a square unit and a parallelogram unit.

starting field. Then we anneal the sample from an initial temperature, for instance, 1 K, to zero. The temperature is dropped to zero in 1000 steps and remains at each step for 2000 molecular dynamic (MD) steps. After the vortex configurations are obtained, we applied a slowly increasing, spatially uniform driving force F^L, which simulates a Lorentz force produced by an applied current in the real experiments. We typically increase the driving force by $0.000\,5f_0$ for every 2000 MD steps for a range of F^L ranging from 0 to $0.6f_0$ in the x direction along a symmetry axis of the periodic pinning array, and measure the average of the velocity as a function of the driving force, writing out the average velocity in the x direction ($\langle v_x \rangle$) every 20 MD steps. This quantity is related to a macroscopic measured voltage-current $V(I)$ curve. The depinning force is defined to be the value at which v_x reaches a threshold value. The principle of measuring the magnetization curve is quite similar to the previous simulation[17] except for the parameters. The sample size used in calculating the magnetization is $36\times96\ \Lambda^2$ and the central region is $36\times72\ \Lambda^2$.

IV. CRITICAL DEPINNING FORCE

The critical depinning forces f_p^c with respect to H/H_1 (up to $H/H_1=1.25$) for three configurations are shown in Fig. 2. We have defined it by the onset of the vortex motion. Here, H_1 is the magnetic field, at which the density of the vortex is equal to the density of magnetic dots. This is actually the first matching field for the FM configuration.[8–11]

A pronounced feature is that f_p^c is asymmetrical with respect to H/H_1 for the FM configuration and essentially symmetrical for the AFM and AFM2×2 configurations. The asymmetric pinning for the FM configuration is similar to that observed in the magnetization measurement.[8–10] In the positive branch $H>0$, several pronounced peaks, as shown in Fig. 2, are seen at the integer and some fractional fields for all three configurations. However, similar peaks are only found in the negative branch for the AFM and AFM2×2 configurations. The different f_p^c behaviors show that different pinning properties can be achieved by changing the configuration of the magnetic dot arrays.

The pronounced asymmetry of pinning properties of the FM array can be qualitatively explained by the field polarity-dependent pinning of the magnetic dots. For the FM configuration [Fig. 2(a)], the vortices are strongly pinned at the pinning sites at $H>0$. But, at $H<0$, the antivortices are repelled by the dots, and are caged at the interstitial positions. However, for the AFM and AFM2×2 configurations, the vortices are pinned at the up-magnetized dots at $H>0$, while at $H<0$ the antivortices are pinned at the down-magnetized dots. This means that independent of the polarity of the field, the field-induced vortices and/or antivortices can always be pinned by the dots with the same orientation of their magnetization. Furthermore, due to the equal density of the up- and down-magnetized dots in our sample, the critical depinning force at a positive field must be equal to that of the corresponding negative field. Hence, the observed symmetrical behavior [Figs. 2(b) and 2(c)] has a rather straightforward origin.

To get a better insight into microscopic origins of the asymmetric and symmetric pinning, vortex patterns at some matching fields are presented in Figs. 3–6 for FM, AFM, and AFM2×2 configurations, respectively. The solid dots are vortices/antivortices, and the black open and gray filled circles are the up- and down-magnetized dots, respectively. Figure 3(a) shows the vortex state for the FM configuration at $H/H_1=1/4$, where the first pronounced peak in Fig. 2(a) is observed. In this case the vortices occupy every other site in every other column. They form an incomplete triangular order. Domain walls (dashed dotted lines) are present in the sample. This can be explained by a small difference in en-

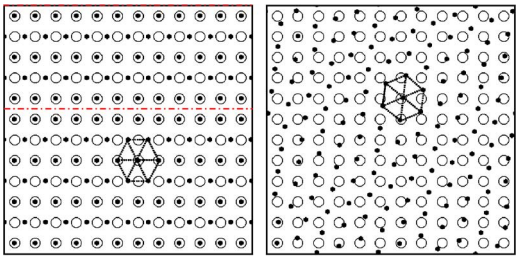

FIG. 4. (Color online) Vortex patterns for the FM configuration at $H/H_1=1$ in (a) intermediate phase, and (b) deformed triangular phase. The black dot lines indicate the triangular vortex lattice and the dashed dotted lines are the domain walls.

ergy between a square unit along the domain walls and a parallelogram unit when the density of the vortices is small. In Fig. 3(b) we show the vortices at $H/H_1=1/2$ which form a checkerboard ordered state. It is completely ordered with a square vortex lattice rotated by 45°. At $H/H_1=1$ [Fig. 3(c)], every pinning site is occupied by a vortex to form a very stable pattern. The common feature of these vortex patterns is that partial or complete matching can be found between the vortex lattice and the magnetic dot array. Figures 3(d)–3(f) show vortex patterns at $H/H_1=-1/4$, $H/H_1=-1/2$, and $H/H_1=-1$, respectively. The antivortices are caged at the interstitial positions because of repulsive interactions between vortices and pinning sites. The obvious difference in vortex states at $H>0$ and $H<0$ yields the asymmetric pinning.

The vortex patterns are known to be dependent on the strength of the pinning sites.[24] The regular triangular vortex lattice has the lowest energy in the absence of any pinning effect. However, in the opposite limit (strong pinning), the

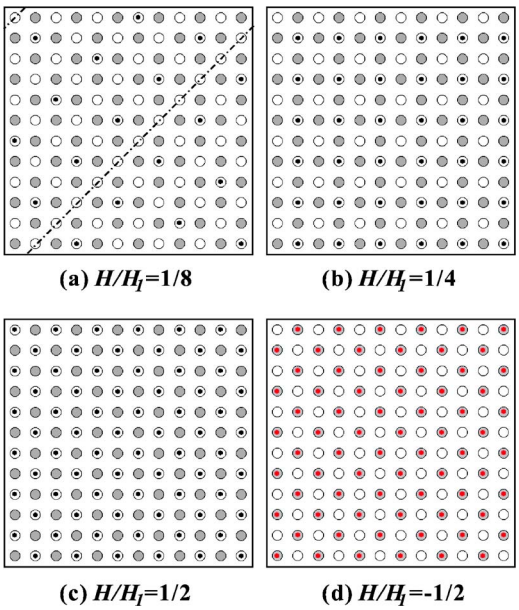

FIG. 5. (Color online) Vortex patterns for the AFM configuration at (a) $H/H_1=1/8$, (b) 1/4, (c) 1/2, and (d) −1/2. The dashed dotted lines indicate the domain walls.

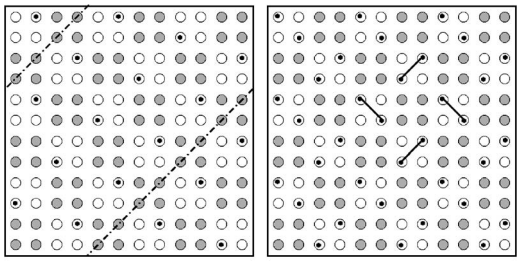

FIG. 6. Vortex patterns for the AFM2×2 configuration at (a) $H/H_1=1/8$ and (b) 2/8. The domain walls and the vortex dimers are indicated by the dashed dotted and solid lines, respectively.

vortex lattice will prefer to follow the lattice imposed by the pinning site array. Therefore, a vortex lattice can exist in the form of at least two stable phases: pinned regular phase and triangular phase. In the case of the first matching field, an intermediate phase can also be found in the corresponding pinning strength. In our simulations, we can also find these three phases. The pinned phase has been shown in Fig. 3(c). When the pinning strength is considerably decreased, e.g., $f_p=0.013f_0$, an intermediate phase can be obtained as shown in Fig. 4(a). Almost half of the vortices are pinned at the sites, and the others sit in the interstitial positions. They form a regular triangular lattice (dotted lines). When the pinned strength is further decreased, e.g., $f_p=0.0028f_0$, the deformed triangular lattice can be seen in Fig. 4(b). Our simulation results are in a good agreement with the data reported in Ref. 24 except for the domain walls (dashed dotted lines) in the intermediate phase [Fig. 4(a)].

For the sample with the AFM configuration, Fig. 5(a) shows the vortex pattern at $H/H_1=1/8$, which is an incompletely ordered lattice with vortices occupying every other pinning site along every other diagonal stripe of the up-magnetized dots. Domain walls (dashed dotted lines) can also be observed in this case as that in the FM configuration. The vortices at $H/H_1=1/4$, as shown in Fig. 5(b), form a square lattice, which is completely ordered. Figure 5(c) shows the vortex lattice at $H/H_1=1/2$. The vortices just occupy completely every up-magnetized dot and the whole vortex pattern is an ordered checkerboard state. We also show in Fig. 5(d) the vortex state at $H/H_1=-1/2$. The antivortex pattern is the same as that at $H/H_1=1/2$, except that the roles of the up-and down-magnetized dots are interchanged. Hence, the symmetrical pinning effect is observed in this case.

Figures 6(a) and 6(b) present the vortex patterns for the AFM2×2 configuration at $H/H_1=1/8$ and 2/8, respectively. At $H/H_1=1/8$ the first pronounced peak in f_p^c is found [Fig. 2(c)]. As shown in Fig. 6(a), the vortices are located alternatively in the bottom-left and top-right corners of every 2×2 up-magnetized subarray in different diagonal strips. Domain walls (dashed dotted lines) are also observed here as in the case of the FM and AFM configurations. In Fig. 6(b) at $H/H_1=2/8$, the vortices arrange themselves in a vortex dimer (solid lines) lattice, where each dimer is stabilized along alternate diagonal directions in every 2×2 up-magnetized subarray. These two figures illustrate that the

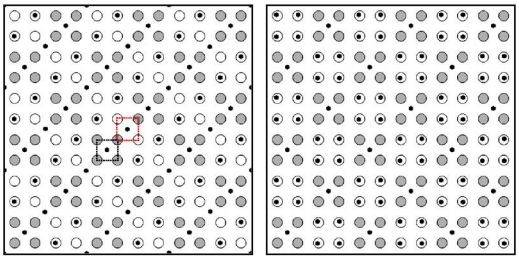

FIG. 7. (Color online) Vortex patterns for the AFM2×2 configuration at (a) $H/H_1=4/8$ and (b) 5/8. The center of the lower (upper) square indicated by dotted lines is the cage (saddle) point.

vortex patterns completely or partly match the available pinning sites. Consequently, the peaks in f_p^c occur due to these matching effects. The vortex pattern at negative values $H/H_1=-1/8$ and $H/H_1=-2/8$ (not shown here) is the same as that at the corresponding positive field values, except that the antivortices are pinned by the down-magnetized dots. Therefore, the symmetrical pinning effect can be obtained, similar to the AFM configuration.

There are two weak features clearly seen in Fig. 2(c) for the AFM2×2 array. The first one is a local f_p^c minimum at $H/H_1=\pm 4/8$. We show the vortex array with the field $H/H_1=4/8$ in Fig. 7(a). One can find that half of the vortices occupy two pinning sites along the diagonal in every 2×2 plaquette with up-magnetized dots. Along the same direction, the other half of the vortices is occupying the interstitial positions. There are two positions for the interstitial vortices. The first one is the position located in the center of every 2×2 magnetic dot subarray with down magnetization (the lower square marked by dotted lines). The vortex is well caged by the dots in the subarray. The second position is in the center of a square (the upper one marked by dotted lines), which is composed of two up-magnetized and two down-magnetized dots. The vortex state in this case is not stable if we only consider the forces from the nearest vortices. For instance, if the vortex deviates from the equilibrium position along the direction connecting two up-magnetized dots, it favors to move farther due to the larger attraction from the nearest up-magnetized dots. Hence, the forces from other dots are necessary to stabilize this vortex. We also notice that the vortex deviating along the direction connecting two down-magnetized dots, will be pushed back due to the larger repulsive force from the nearest down-magnetized dot, and therefore will favor to stay at the equilibrium position. So, this position is actually a saddle point.[1] This means that such interstitial vortices are relatively easily depinned, and therefore the critical depinning force at this field is expected to be relatively small. Meanwhile, no more vortices can occupy the interstitial positions around this field; therefore, a localized minimum is formed at this field.

The second weak feature is a set of several consecutive peaks appearing in the region of $4/8<H/H_1<8/8$, which leads to the increased level of the average f_p^c over this region, in contrast to the corresponding region for the AFM configuration. This can be explained by the formation of several ordered states at $H/H_1=5/8$, 6/8, 7/8, and 8/8. Figure 7(b), as an example, shows the vortex distribution at $H/H_1=5/8$. The vortex density at this field is higher than the density of up-magnetized dots. Hence, all the ferromagnetic dots are occupied by the vortices. The remaining vortices are well caged by down-magnetized dots in the interstitial positions. All vortex-vortex and vortex-pinning center interaction forces acting on a vortex sitting there will cancel each other to form a stable position. This stable position can be considered as a virtual attractive pinning center. Consequently, f_p^c is increased.

One of the motivations of studying the f_p^c behavior is to find a way to increase the critical current density of a superconductor, J_c, which corresponds to f_p^c in the simulation, i.e., the larger f_p^c the higher J_c. Figure 2(d) shows that at the matching fields the maximum f_p^c value for the AFM configuration is $0.283f_0$, which is a bit higher than the largest pinning strength $f_p=0.279\,22f_0$ provided by a single (isolated) magnetic dot. But for the FM configuration it decreases to $0.276f_0$, which is a bit lower than f_p. This difference can be qualitatively explained as follows. First, we will neglect the long-range interaction between the vortices because these forces, due to the symmetry, cancel each other at the matching field. Second, due to the size effect of the magnetic dots, we cannot cancel out the interactions from the neighboring dots. Since the cut off length for the vortex-pinning site interaction in our simulations is equal to the lattice parameter a, we only consider the nearest-neighbor site in the direction of the vortex motion. For the FM configuration, the nearest-neighbor site attracts the pinned vortex and causes the vortex to be depinned more easily than a vortex pinned at an isolated site. Hence, the maximum of the critical depinning force for the FM configuration is a bit lower than that for an isolated vortex f_p. However, for the AFM configuration, the nearest-neighbor site of every pinned vortex at the matching fields is a down-magnetized dot. Due to the repulsive interaction between this dot and the pinned vortex, the nearest neighbor will push the pinned vortex back to the pinning site, thus causing the vortex to be depinned less easily than a vortex pinned at an isolated site. Therefore, the maximum of the critical depinning force for the AFM configuration is somewhat higher than f_p. This indicates that the critical current J_c can be increased when the down-magnetized dots are introduced and the dot size effect is considered. Although the increment is small, we believe that a higher J_c value could be achieved by optimizing the physical parameters in the AFM dot array.

V. MAGNETIZATION

In Fig. 8 we show the magnetization curves (magnetization M versus H/H_1) up to $H/H_1=2.5$ for three configurations of the magnetic dot array. For the FM configuration, an asymmetric magnetization curve is clearly seen in Fig. 8(a). At positive field $H>0$, peaks and cusps are distinctly visible not only at integer fields $H/H_1=2$ and 1 but also at the fractional fields 1/2 and 2/3. But at negative fields, where the pinning potential is repulsive, no matching features are present. Figure 8(b) shows the comparison of our simulation with the experiment,[25] which measured the $M(H)$ of a super-

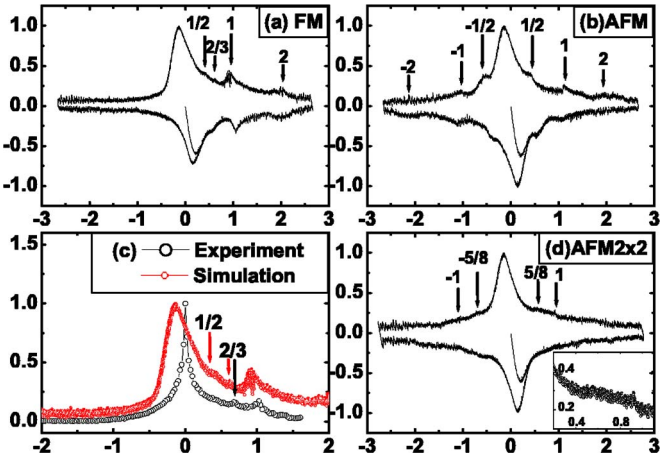

FIG. 8. (Color online) (a) Magnetization curve for the FM configuration with $H/H_1<2.5$. The curve is clearly asymmetrical. The slight shift of the upper branch to lower field values and the lower branch to higher field values is caused by the high field sweep rate during the simulations. (b) A comparison between the simulation and experiment for the FM configuration. (c) and (d) are the magnetization curves for the AFM and AFM2$\times$2 configurations, respectively. They are obviously symmetrical. Some strong and weak peaks indicating the matching and submatching field are labeled. The inset in (d) shows the weak enhancement of the f_p^c values at $4/8<H/H_1<8/8$.

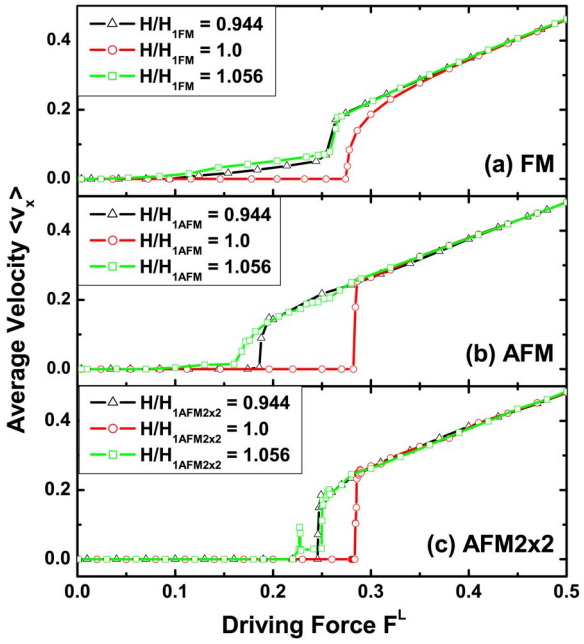

FIG. 9. (Color online) The average velocity of vortices in the x direction versus the driving force F^L at both commensurate and incommensurate fields for the (a) FM, (b) AFM, and (c) AFM2$\times$2 configurations.

conducting Pb film on top of a magnetic dot Co/Pt array at temperature $T=7.18$ K. The experimental and theoretical data are in good agreement with each other. They are both asymmetrical: low magnetization with no matching effects at negative fields and high magnetization with strong or weak matching effects at positive fields. It should be noted that the upper (lower) branch of the simulation curve is slightly shifted to lower (higher) field values. This is caused by the high field sweep rate during the simulations.

However, for the AFM configuration in Fig. 8(c), due to the equal density of the up- and down-magnetized dots, the $M(H)$ curves are almost symmetrical. The matching effects are seen at $H/H_1=\pm1/2$, ±1, and ±2. We can also find the symmetric feature for the AFM2$\times$2 configuration, as shown in Fig. 8(d), together with weak peaks at both $H/H_1=\pm5/8$ and ±1. The inset in Fig. 8(d) shows a weak enhancement at $4/8<H/H_1<8/8$ which is in agreement with the relatively high f_p^c values discussed in Sec. IV.

VI. CURRENT-VOLTAGE CHARACTERISTICS

In this section, we will discuss the average velocity of vortices in the x direction, $\langle v_x\rangle$, versus the driving (Lorentz) force F^L, which corresponds to the current-voltage (I-V) characteristics of the thin SC film. Before analyzing the results of our calculations we should briefly comment on the definition of the first matching field. Obviously, the H_1 definition for the FM configuration mentioned above is not applicable to the AFM and AFM2$\times$2 configurations because a vortex cannot occupy the down-magnetized dots when $H>0$ and an antivortex cannot occupy the up-magnetized pinning sites when $H<0$. In our calculations for the AFM array, we define the first matching field as the one at which the density of the vortices is equal to the density of the unit cells. For this new definition, the first matching field for the FM configuration can be kept unchanged, while for the AFM and AFM2$\times$2 configurations, denoted by H_{1AFM} and $H_{1AFM2\times2}$, respectively, the values are equal to $1/2H_1$ and $1/8H_1$. In the following, H_{1FM} is also used to denote the first matching field for the FM configuration.

Figure 9 shows a series of the I-V curves for all three configurations at fields 0.944, 1.0, and 1.056 (in units of the corresponding first matching field). At the matching fields, only a single voltage jump is observed for each configuration. This indicates that all vortices are depinned simultaneously. An obvious distinction in the transition from the pinned phase to the finite moving phase between FM and AFM as well as AFM2$\times$2 can be found in the figure. It means that a continuous transition occurs for the FM configuration, but a discontinuous one for the AFM and AFM2$\times$2 configurations. This difference is caused by the different trajectories of the depinned vortices. Figures 10(a) and 10(b) show the trajectory lines of the moving vortices at $F^L=0.284f_0$ for the FM and AFM configurations, respectively. In Fig. 10(a), all the vortex motion is restricted to the 1D channels along the pinning site rows, which is similar to the previous simulations.[15,16] In this case, the vortex-pinning site interaction force will balance F^L, yielding a gradual increase in the $\langle v_x\rangle$ with respect to F^L. However, for the AFM configuration at the same F^L, two kinds of the trajectories appear in the sample: spindle lines along the pinning site rows and sinusoidal lines along the channels between two adjacent pinning site rows, as seen in Fig. 10(b). When vortices move along any of these two kinds of the trajectories, the vortex-

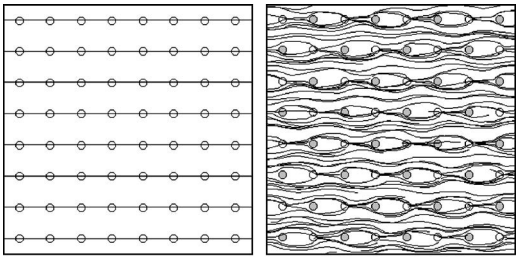

(a) *FM* (b) *AFM*

FIG. 10. Vortex trajectories at the first matching field with $F^L = 0.284 f_0$ for the (a) FM configuration and (b) AFM configuration. Spindle and sinusoidal trajectories are found. The vortex-pinning site interaction forces decreased greatly.

pinning site interaction forces in the x direction will decrease greatly. These forces are so weak that they cannot balance the F^L. Thus, the average velocity of the vortices in the x direction can reach higher values in a very narrow range of F^L just beyond f_p^c, and then almost linearly increase with F^L.

At incommensurate fields, different I-V curves are displayed for the three configurations. For the FM configuration at $H/H_{1FM}=0.944$ and 1.056, respectively, a two-stage depinning process takes place as shown in Fig. 9(a). The initial response is due to the depinning of the interstitial vortices, and the second larger jump occurs when all the vortices begin to move.[15,16] It should be noted that the interstitial vortices at $H/H_{1FM}=0.944$ are induced by some of the vacancies due to the presence of the pinning which is not strong enough. Figure 11(a) shows the stable vortex state just after annealing. The nearest pinned vortices from an interstitial position form a hexagon (dotted lines). Hence, the center of the hexagon should be an equilibrium position, in which interstitial vortices are favored. The long-range vortex-vortex repulsive interaction forces the vortices to stay in these positions when the perturbation is applied. We also give the I-V curves for the AFM configuration in Fig. 9(b). A two-stage depinning process is observed again at $H/H_{1AFM}=1.056$ as that found for the FM configuration. However, only the single jump is found at $H/H_{1AFM}=0.944$. This is because the vacancies in this case cannot induce the interstitial vortices. The repulsive interactions from the neighboring sites do not allow vortices to occupy the interstitial positions, as shown in Fig. 11(b). For the AFM2$\times$2 configuration, the I-V curves are similar to those for the AFM configuration except for a considerable velocity oscillations in the region $F^L=0.227f_0$–$0.228f_0$ and a velocity plateau in the curve for $H/H_{1AFM2\times2}=1.056$ in Fig. 9(c). In the velocity oscillation region we find that most of the vortices are depinned and are moving in a random manner, which leads to a sharp increase in $\langle v_x \rangle$. However, in the range $0.228f_0-0.250f_0$, some of the moving vortices are repinned by the up-magnetized dots and the others are just moving along or between the pinning site rows, thus yielding a velocity plateau with increasing F^L. The above two regions are similar to the regions III and IV, respectively, discussed in Ref. 15 for a system with an antidot array.

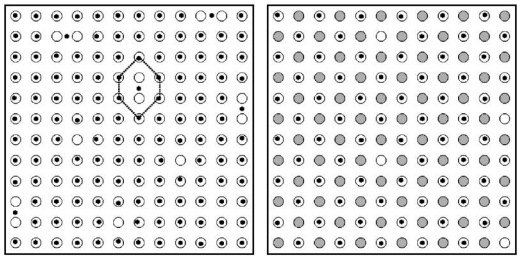

(a) $H/H_{1FM}=0.944$ (b) $H/H_{1AFM}=0.944$

FIG. 11. (a) Vortex pattern for the FM configuration at $H/H_{1FM}=0.944$. With not very strong pinning strength, part of the vacancies induce the interstitial vortices, which are stably caged at the centers of hexagons (dotted lines). (b) Vortex pattern for AFM configuration at $H/H_{1AFM}=0.944$. No interstitial vortices occur in this configuration.

VII. CONCLUSIONS

We have simulated the pinning properties and the vortex dynamics in thin SC film with different regular arrays of magnetic dots. Three kinds of magnetic dot arrays, FM, AFM, and AFM2$\times$2 were investigated. By taking advantage of the field polarity-dependent pinning effect, we successfully tuned pinning from asymmetric (FM) to symmetric (AFM and AFM2$\times$2) with pronounced matching effects. Moreover, we have shown that the critical current of the SC film can be enhanced by using the AFM configuration of magnetic dots.

The vortex dynamics was also studied in this paper. We presented a series of the I-V curves for three configurations of magnetic dots at both commensurate and incommensurate fields. At the first matching field, the I-V curves demonstrate a continuous transition to the vortex moving region for the FM configuration, while discontinuous transition for the AFM and AFM2$\times$2 configurations. This can be explained by the difference in the vortex dynamical trajectories in these pinning arrays.

ACKNOWLEDGMENTS

This work was supported by the Research Fund K.U. Leuven GOA/2004/02, the Belgian Interuniversity Attraction Poles (IUAP), and the Flemish FWO programs. Helpful discussions with Clécio C. de Souza Silva, and B. Y. Zhu are gratefully acknowledged.

*Electronic address: Victor.Moshchalkov@fys.kuleuven.be

[1] M. Baert, V. V. Metlushko, R. Jonckheere, V. V. Moshchalkov, and Y. Bruynseraede, Phys. Rev. Lett. **74**, 3269 (1995); V. V. Moshchalkov, M. Baert, V V. Metlushko, E. Rosseel, M. J. Van Bael, K. Temst, R. Jonckheere, and Y. Bruynseraede, Phys. Rev. B **54**, 7385 (1996); V. V. Moshchalkov, M. Baert, V. V. Metlushko, E. Rosseel, M. J. Van Bael, K. Temst, Y. Bruynseraede, and R. Jonckheere, *ibid.* **57**, 3615 (1998).

[2] K. Harada, O. Kamimura, H. Kasai, T. Matsuda, A. Tonomura, and V. V. Moshchalkov, Science **274**, 1167 (1996).

[3] A. Castellanos, R. Wördenweber, G. Ockenfuss, A. v. d. Hart, and K. Keck, Appl. Phys. Lett. **71**, 962 (1997).

[4] A. N. Grigorenko, G. D. Howells, S. J. Bending, J. Bekaert, M. J. Van Bael, L. Van Look, V. V. Moshchalkov, Y. Bruynseraede, G. Borghs, I. I. Kaya, and R. A. Stradling, Phys. Rev. B **63**, 052504 (2001).

[5] B. Y. Zhu, L. Van Look, V. V. Moshchalkov, B. R. Zhao, and Z. X. Zhao, Phys. Rev. B **64**, 012504 (2001).

[6] J. I. Martin, M. Velez, J. Nogues, and Ivan K. Schuller, Phys. Rev. Lett. **79**, 1929 (1997).

[7] D. J. Morgan and J. B. Ketterson, Phys. Rev. Lett. **80**, 3614 (1998).

[8] M. J. Van Bael, M. Lange, S. Raedts, V. V. Moshchalkov, A. N. Grigorenko, and S. J. Bending, Phys. Rev. B **68**, 014509 (2003).

[9] M. J. Van Bael, Physica C **332**, 12 (2000).

[10] M. Lange, M. J. Van Bael, L. Van Look, K. Temst, J. Swerts, G. Güntherodt, V. V. Moshchalkov, and Y. Bruynseraede, Europhys. Lett. **53**, 646 (2001).

[11] A. N. Grigorenko, S. J. Bending, M. J. Van Bael, M. Lange, V. V. Moshchalkov, H. Fangohr, and P. A. J. de Groot, Phys. Rev. Lett. **90**, 237001 (2003).

[12] C. Reichhardt, C. J. Olson, J. Groth, S. Field, and F. Nori, Phys. Rev. B **53**, R8898 (1996).

[13] C. Reichhardt, J. Groth, C. J. Olson, S. B. Field, and F. Nori, Phys. Rev. B **54**, 16108 (1996).

[14] C. Reichhardt, C. J. Olson, and F. Nori, Phys. Rev. B **57**, 7937 (1998).

[15] C. Reichhardt, C. J. Olson, and F. Nori, Phys. Rev. B **58**, 6534 (1998).

[16] C. Reichhardt and N. Gronbech-Jensen, Phys. Rev. B **63**, 054510 (2001).

[17] G. Teniers, M. Lange, and V. V. Moshchalkov, Physica C **369**, 268 (2002).

[18] J. Pearl, Appl. Phys. Lett. **5**, 65 (1964).

[19] E. Olive and E. H. Brandt, Phys. Rev. B **57**, 13861 (1998).

[20] E. Olive and E. H. Brandt, Phys. Rev. B **59**, 7116 (1999).

[21] H. Fangohr, A. Price, S. Cox, P. A. J. de Groot, G. J. Daniell, and K. S. Thomas, J. Comput. Phys. **162**, 372 (2000).

[22] Hans Fangohr, Simon J. Cox, and Peter A. J. de Groot, Phys. Rev. B **64**, 064505 (2001).

[23] M. V. Milosevic and F. M. Peeters, Phys. Rev. B **68**, 094510 (2003).

[24] W. V. Pogosov, A. L. Rakhmanov, and V. V. Moshchalkov, Phys. Rev. B **67**, 014532 (2003).

[25] M. J. Van Bael, M. Lange, and V. V. Moshchalkov (private communication).